Publicado en Phys. Chem. Chem. Phys. 4 (2002) 149-159 (DOI: 10.1039/b106765f)

Effects of thermal pre-treatments on the redox behaviour of $Ce_{0.5}Zr_{0.5}O_2$: isotopic and spectroscopic studies

P. Fornasiero[a], T. Montini[a], M. Graziani[a], J. Kašpar[a,*], A.B. Hungría[b], A. Martínez-Arias[b], J.C. Conesa[b,*]

[a]Dipartimento di Scienze Chimiche, Università di Trieste, via Giorgieri 1, 34127 Trieste, Italy.
E-mail: kaspar@univ.trieste.it

[b]Instituto de Catálisis y Petroleoquímica, CSIC. Campus de Cantoblanco, 28049 Madrid, Spain.
E-mail: jcconesa@icp.csic.es

The temperature programmed reduction (TPR) of a single phase $Ce_{0.5}Zr_{0.5}O_2$ solid solution is investigated by using $^1H_2$/Ar and $^2H_2$/Ar mixtures as reducing agents. The effects of mild (700 K) or severe (1273 K) preoxidation (MO, SO) on the TPR profile are analysed. It is observed that after SO pretreatment hydrogen activation/scrambling occurs at about 600 K and the reduction profile is characterised by a single reduction peak at 920 K. In contrast, a TPR/MO pretreatment of such SO sample leads to a facile hydrogen activation/scrambling and low temperature reduction profiles, the main reduction peak being observed at ca. 650 K. Using $^1H_2$ and $^2H_2$ as reducing agents, an isotopic effect is observed for the reduction processes with a peak occurring above 700 K, while equal activation energies are measured for those occurring below 700 K. This suggests that under the TPR conditions the surface reduction steps (activation of the reducing agent at the surface, surface reduction steps and water evolution) are not rate limiting for the low temperature reduction process, which is controlled by bulk diffusion, while some surface step (probably water formation) is limiting for the high temperature reduction. Studies by EPR on the nature of the oxygen species adsorbed on variously pretreated specimens and by FTIR of the methoxy species formed upon methanol adsorption on the same materials reveal that the main changes induced by high temperature calcination are related to segregation of ceria- and zirconia-type islands, with some surface enrichment in cerium probably occurring as well. Only subtle differences between SO and MO pretreated samples can be detected at either surface or bulk (XRD experiments) levels, in contrast with the significant modifications produced by the different pretreatments on the reduction characteristics of the sample.

1. Introduction

The so-called oxygen storage/release capacity (OSC) of a three-way catalyst (TWC) is the ability to attenuate the negative effects rich/lean oscillations of exhaust gas composition. By maintaining a stoichiometric gas composition at the catalyst, the highest efficiency of

modern TWCs is achieved by adding a CeO_2-ZrO_2 mixed oxide component,[1] is usually discussed in terms of the ability to regulate the oxygen partial pressure in the exhaust through the Ce^{3+}/Ce^{4+} redox couple:

$$CeO_2 \underset{H_2O/CO_2}{\overset{H_2/CO}{\rightleftharpoons}} CeO_{2-x} + x/2\ O_2$$

Both H_2 and CO are present in the exhaust in a ratio 1:3, which makes investigation of the reduction process, using either CO or H_2 as reducing agent, of strong interest. Recently a number of investigations concerning reactions of CO with CeO_2-ZrO_2 mixed oxides which are related to the OSC property as described above appeared in the literature.[2] CO oxidation was investigated under oscillating or constant feed-stream composition, or even in the absence of O_2 , due to its relevance to the OSC property. We have investigated in detail the redox behaviour of these materials using H_2 as reducing agent and showed that promotion of the redox behaviour of these systems could be related to structural modification of the CeO_2 lattice by insertion of ZrO_2, which makes the lattice oxygen highly mobile.[3] Evidence from these studies indicated that the reduction of CeO_2, which is a slow process in comparison to CeO_2 oxidation, could be rate limited by the mobility of the oxygen in the bulk. This proposal has been questioned, with the suggestion that processes other than those occurring in the bulk are rate limiting in the reduction process, even at low temperatures.[2] There is a further point of interest in the redox-behaviour of the CeO_2-ZrO_2 mixed oxides, since it has been observed that high temperature reduction followed by mild oxidation leads to unusual improvements in the reduction behaviour at low temperatures.[4] However, this behaviour is reversed by severe oxidation which moves the onset of the reduction processes to high temperatures.[5] An understanding of the reduction mechanism at low temperatures, using H_2 as reducing agent, is desirable since it was shown recently that H_2 can contribute efficiently to OSC property, even at room temperature.[6]

In order to elucidate further these points, we report here temperature programmed reduction experiments carried out on a mixed oxide using both $^1H_2$/Ar and $^2H_2$/Ar mixtures as reducing agents. The changes in the surface state induced by the different pretreatments are probed by O_2 adsorption at room temperature, using EPR technique. Recent studies showed the validity of this technique for evaluation of the type and intensity of superoxide radicals generated upon oxygen adsorption on the outgassed samples, whose presence is directly related to surface reducibility in the CeO_2-ZrO_2 mixed oxides.[7] The studies on surface properties are complemented by infrared experiments using methanol as probe molecule. This method is based on monitoring the methoxy species formed upon methanol adsorption, which gives valuable information on the surface characteristics of this kind of material.[8] A preliminary report on the TPR experiments described here appeared previously.[9]

2. Experimental

$Ce_{0.5}Zr_{0.5}O_2$, with a BET surface area of 40 $m^2\ g^{-1}$, was prepared by using a citrate route, as reported previously.[10] Water was used as solvent. This sample, which was calcined at 773 K for 5 h, is designated as

fresh. The sample was characterised by powder XRD using a Siemens Kristalloflex Mod.F Instrument with Ni-filtered Cu-Kα radiation.

The TPR/oxidation experiments were carried out as follows: the mixed oxide was pretreated in situ in flowing Ar at 873 K for 2 h, while pulsing pure O_2 (100 ml) every 30 s. Such a cleaning pretreatment ensures a clean CeO_2-ZrO_2 surface, providing TPR profiles free from artifacts due to adsorbed species.[11] Notice that water is desorbed by about 500 K. The sample was then cooled in Ar flow to room temperature (RT), the flow switched to either 5% $^1H_2$ or 5% $^2H_2$ in Ar and the temperature ramped at rates of 10-20 K min^{-1} up to 1273 K. The sample was held at this temperature for 15 min, then the gas was switched to Ar and the sample cooled to 700 K, whereupon it was re-oxidised by pulsing pure O_2 (100 ml) every 30 s for 60 min. This treatment is described as mild oxidation (MO). O_2 uptake was also measured during MO by detecting the breakthrough point. The sample was then cooled to RT before a subsequent TPR run was carried out. In some experiments a severe oxidation (SO), i.e. in situ treatment in Ar at 1273 K for 2 h, while pulsing pure O_2 (100 ml) every 30 s, was carried out before cooling the sample to RT. To ensure the reproducibility of the experimental conditions, all the pretreatments, post-treatments and the $^1H_2$ TPR and $^2H_2$ TPR were carried out in situ, on the same sample. H_2 consumption was detected either by a conventional thermal conductivity detector (TPR/TCD) or by using a VG Sensorlab quadrupole mass spectrometer with PostSoft analysis software (TPR/MS). 25 mg of sample was employed in the TPR/TCD experiments, while 200 mg had to be employed for the TPR/MS. In the former case H_2 (5%) in N_2 mixtures was also employed. High purity (99.999%) gases with no further purification were employed. However, due to ubiquitous water and long experimental times, we always detected the presence of ^1H derived products in the TPR/MS experiments carried out with $^2H_2$, as also evidenced by the presence of a peak at m/z=3.

EPR spectra were recorded, always at 77 K, with a Bruker ER 200 D spectrometer operating in the X-band and calibrated with a DPPH standard (g=2.0036). Portions of about 30 mg of sample were placed inside a quartz probe cell with greaseless stopcocks using a conventional high vacuum line (capable of maintaining a dynamic vacuum of ca. 0.006 N m^{-2}) for the di fferent. tSamples outgassed at T_v=773 K were analysed. Oxygen adsorption experiments were performed by adsorbing a dose of ca. 100 mmol of O_2 per g of sample at 77 K. Then, after about 10 min contact, the sample was outgassed for 30 min at 77 K in order to minimise magnetic interactions with non-chemisorbed oxygen (this experiment will be hereafter referred to as oxygen adsorption at 77 K). The experiment was followed typically by warming to RT and finally outgassing at RT for 15 min. In cases where intensity losses were noticed upon warming to RT, the evolution of the signals during the warming process was examined at di fferent warming times.

Infrared spectra were recorded at RT with a Nicolet 5ZDX FTIR spectrometer. Self-supporting discs of the samples (containing 10-15 mg cm^{-2}) were prepared and handled with a conventional static IR cell. Methanol adsorption (50 Torr) was performed at RT on samples previously outgassed at 773 K, followed by outgassing at RT for 15 min and finally outgassing at 373 K for 15 min.

3. Results and discussion

3.1. Bulk structural characteristics of the $Ce_{0.5}Zr_{0.5}O_2$ solid solution

To avoid as far as possible artifacts due to phase separation under the redox-ageing conditions, a single phase $Ce_{0.5}Zr_{0.5}O_2$ solid solution was prepared, which was characterised by XRD, as reported recently.[12] Accordingly we will summarise only the most important features relevant to this study. Powder XRD patterns of the fresh, calcined (1273 K, 5 h) and redox-aged $Ce_{0.5}Zr_{0.5}O_2$ showed no observable splitting of the (222) and (220) reflections, indicating the presence of a fluorite type cation lattice without detectable tetragonal distortion. By using a Rietveld profile fitting of the XRD patterns the cell parameter was calculated as 5.2969(8) Å and the particle size as 12 nm for the $Ce_{0.5}Zr_{0.5}O_2$ calcined at 1273 K for 5 h. A redox-aged sample, i.e. subjected to TPR/MO and TPR/SO treatments as described in the Experimental section, was also analysed to check for structural modifications which could be induced by such an ageing procedure. It was observed that only negligible structural changes of the solid solution were induced by the redox-ageing: the cell parameter was calculated as 5.2816(8) Å and the particle size as 13 nm in the redox aged sample. The Raman spectrum of the fresh $Ce_{0.5}Zr_{0.5}O_2$ sample featured a strong broad band centred at 478 cm^{-1} with a shoulder at about 540 cm^{-1} and weak bands at 310 and 125 cm^{-1}. This allowed attribution to a t'' phase according to the classification proposed by Yashima et al.[13] The intensity of the Raman bands increased somewhat after calcination at 1273 K, which is consistent with an increase in the particle size of the mixed oxide.[14] In agreement with previous studies, upon redox-ageing the Raman spectrum appeared perturbed and the overall intensity of the Raman bands decreased.[15]

3.2. Spectroscopic studies of surface properties

In order to examine surface properties, analyses were carried out with EPR and FTIR, using respectively oxygen and methanol as probe molecules,[7] on the fresh sample and on samples previously subjected to a SO treatment and to SO followed by TPR/MO treatment, indicated respectively as SO and MO samples. As shown below (Section 3.3), the SO and MO sample show distinct reduction behaviour, as most of the reduction occurs respectively above and below 700 K.

Following an outgassing treatment at T_v=773 K, only a very weak symmetric signal at g=2.002 (signal A) is observed in the EPR spectrum of the fresh sample (data not reported). This signal appears typically on ceria-related materials after outgassing at relatively high T_v (673 K) and can be most likely attributed to the generation of a small amount of particular anion vacancy defects at surface or subsurface positions in which single electrons are largely stabilised, according to their weak interaction with oxygen.[16] Di fferent signa
appear after oxygen adsorption at 77 K on the fresh sample outgassed at T_v=773 K, the spectrum remaining unchanged upon subsequent warming to RT for 12 h. Higher spectral intensity and better resolution of the signals formed is however obtained after subsequent outgassing at RT, which is likely attributed to the existence of magnetic interactions between the chemisorbed radicals and some residual non-chemisorbed

oxygen species before this latter outgassing. The spectrum so obtained (Fig. 1(a)) is mainly formed by the overlapping of two signals, designated as OC1 and OZ, a minor signal designated as OC2 being also present. Table 1 shows a summary of the spectral characteristics of these oxygen-derived signals.

Certain similarities are observed in the nature and evolution of the EPR oxygen-derived signals detected on samples MO and SO during the various oxygen adsorption experiments. After outgassing at T_v=773 K, a signal A larger than that observed on the fresh sample (by factors of about 5 and 16 for samples MO and SO, respectively) is detected in both specimens, Fig. 1(b) and (e). The spectra observed for both samples after subsequent O_2 adsorption at 77 K, Fig. 1(c) and (f), suggest the presence (apart from a small signal A, representing always an amount of spins below 0.1% of the total) of overlapped, relatively broadened signals with an overall intensity slightly higher for sample SO. (In relative terms, the intensities observed for the fresh, MO and SO samples, spectra in Fig. 1(a), (c) and (f), are respectively 1, 0.79 and 1.05.) Careful analysis by computer simulation of these spectra is shown in Fig. 2; it allows us to verify that they are formed by a superposition of two signals OC1' and OC2, su fficiently di larger linewidth and less accurately determined parameters; these latter are included in Table 1. The main di ference between the spectra of th OC2/OC1'=3.5/1 for MO and 3/2 for SO (as obtained from doubly integrated intensities of the best-fit spectra: note that the change in signal amplitude ratio is somewhat di ferent due to variations i remarkable that no hint of signal OZ appears in the EPR experiments performed on these samples, in contrast to the fresh sample (Fig. 1(a)).

For both samples MO and SO, and in contrast to the behaviour observed on the non-sintered fresh sample, a significant decrease and eventual disappearance of the signals is observed upon subsequent warming to RT (Fig. 3); this cannot be attributed to magnetic broadening e fects of bound oxygen since no intensity recovery is observed after subsequent RT outgassing. It is noteworthy that similar behaviour, in terms of the type and shape of the signals present and their evolution during warming to RT, has been observed on a pre-sintered (by calcination under air at 1273 K for 12 h) pure ceria reference sample (experiments not shown), again contrasting with the behaviour of high surface area ceria.[16] In general terms, it is observed that the intensity decrease upon warming to RT a fects signa OC1', as inferred from analyses of the spectra shown in Fig. 1(d) and (g) compared to those observed after O_2 adsorption at 77 K (Fig. 1(c) and (f)). Following the complete loss of these oxygen-derived signals after prolonged warming to RT, a second (and a third in the case of sample SO) oxygen dose was adsorbed at 77 K, followed by similar warming to RT. With these successive doses of oxygen, the spectra observed after adsorption at 77 K show similar signals as above but with progressively smaller overall intensity, while the signal intensity decrease observed upon subsequent warming to RT also becomes slower.

Signals type OC1 (OC1 and OC1') and OC2 are typical of O_2^- species adsorbed on coordinatively unsaturated Ce ions (cus-Ce, formally in the Ce^{4+} state).[7] According to previous work, the di fferences ob these signals with respect to their EPR parameters and to the thermal preconditioning required for their

generation reveal the di fferent natu

vacancies and associated anion vacancies for signals type OC1 and OC2 respectively.[16] These assignments have been supported by NO adsorption experiments showing that only the latter type of defect has NO reduction activity (yielding N_2O) at low temperature;[17] the presence of associated vacancy defects on single crystal ceria surfaces has also been evidenced experimentally by scanning tunnelling microscopy (STM).[18] Signal OZ, on the other hand, is attributed to O_2^-–Zr^{4+} species.[7,19] Formation of the superoxide species requires prior generation of both surface oxygen vacancies, where oxygen may become adsorbed, and excess electrons, which may be transferred (to O_2) from the sample surface. Considering that the reduction of cerium cations, as well as the generation of surface anion vacancies, can be achieved by the outgassing treatment, the formation of O_2^--Ce^{4+} can be envisaged as process:

$$O_2 + V_{ö}\text{-}Ce^{3+} \rightarrow O_2^-\text{-}Ce^{4+}$$

where $V_{ö}$ denotes a doubly ionised oxygen vacancy. More doubts exist concerning the mechanism of formation of the O_2^-–Zr^{4+} species, due to the considerably lower reducibility of Zr^{4+} which makes less likely the presence of Zr^{3+}.[20] A possibility is that oxygen is first chemisorbed on the more reducible cerium cations, the resulting O_2^- radicals being then transferred to zirconium cations where the superoxide species are finally stabilised.[7] Formation of O_2^--Zr^{4+} evidences, in any case, the generation of oxygen vacancies in the coordinative environment of Zr^{4+} cations.

The formation of a large amount of O_2^--Zr^{4+} species upon oxygen adsorption on the fresh sample, which contrasts with similar experiments on high surface area pure zirconia where very small amounts of such species appeared,[11] evidences the promoting eff ect of cerium cations on the generation of vacancies in the coordinative environment of zirconium cations, suggesting that a mixed oxide-type morphology is present at the surface of that sample. This same characteristic was also detected in other $Ce_{0.5}Zr_{0.5}O_2$ specimens of high homogeneity prepared by the microemulsion method,[7] and can be considered demonstrative of the mixed oxide character of the sample surface. In contrast, the absence of O_2^-–Zr^{4+} in the experiments performed here on samples MO or SO indicates the lack of the influence of the cerium component in enhancing vacancy formation on zirconium cations, suggesting that the mixed oxide character of the topmost surface is lost as a consequence of the high temperature thermal treatments. This might be due either to the absence of zirconium cations at the outermost surface layer (induced by a process of cerium segregation to the surface) or to the formation of zirconia islands of low reducibility coexisting with Zr-free ceria islands. The data show in any case that significant surface structure modifications are produced by the high temperature treatments. On the other hand, the decrease in the superoxide signals upon warming to RT in both samples MO and SO, which contrasts with the stability of such species in the fresh sample and reveals the higher facility of reoxidation of the surface vacancies created on these sintered materials, indicates that a higher overall reduction degree is achieved at their surface upon outgassing at T_v=773 K. Accordingly, considering the general scheme of oxygen reduction/surface reoxidation

$$O_2 \rightarrow O_2^- \rightarrow O_2^{2-} \rightarrow 2O^- \rightarrow 2O^{2-}$$

the observation that, upon adsorption of successive oxygen doses on the samples, the amounts of O_2^--Ce^{4+} species diminish and their decrease with warming to RT becomes slower is consistent with the gradual oxidation of the sample surface. In this respect, the higher decrease in signal OC2 with respect to signal OC1' upon warming to RT indicates, in agreement with previous results, that associated oxygen vacancies are more easily oxidised than isolated ones.[16]

FTIR spectra in the C–O bond stretching region obtained following methanol adsorption on the samples outgassed at T_v=773 K are shown in Fig. 4. The spectrum of the fresh sample is formed by bands at 1153, 1097 and 1058 cm^{-1} (Fig. 4(a)). A considerable intensity decrease is observed in the spectra of samples MO and SO, in correlation with their lower surface area (Fig. 4(b) and (c)). In both cases, the spectra show bands at 1157, 1102-1098 (with a shoulder at ca. 1120 cm^{-1}), 1073-1070 and 1027 cm^{-1}. The main di fference between the spectra of the two samples concerns the relative intensity of the band at ca. 1070 cm^{-1}, which is considerably higher for sample MO.

According to previous studies, these bands are attributed to the ν(OC) stretching mode of methoxy species generated upon dissociative methanol adsorption.[8] The frequencies of these bands are sensitive to the nature and redox state of the cations exposed at the surface where methoxy species are chemisorbed, and thus serve as a powerful tool for surface analysis.[8]

Following those studies, bands at 1157-1153 cm^{-1} and at 1102-1097 cm^{-1} are attributed to on-top methoxy species adsorbed, respectively, on Zr^{4+} and Ce^{4+} cations,[8] while the shoulder at ca. 1120 cm^{-1} is attributed to on-top species adsorbed on Ce^{3+} cations.[21] Bands at 1058 cm^{-1} and 1073-1070 cm^{-1} are attributed to doubly bridging methoxy species;[8] for these complexes, the similarities in the frequencies observed for these bands in pure ceria and zirconia in comparison with the present ceria-zirconia mixed oxide samples make unreliable any attempt to determine the exact nature of the two cations presumably involved in the bonding, although the blue shift of the latter bands is a clear indication that the corresponding cerium cations are, on average, in a more reduced state.[22] Finally, the band at 1027 cm^{-1} is related to triply bridging methoxy species.[8] This band is absent in pure zirconia; over oxidised pure ceria, it appears at around 1013 cm^{-1} [8] and shifts to higher frequency as the degree of reduction of ceria is increased.[22]

On the basis of these attributions, it is possible to conclude that one di fference bet
fresh sample and those of the MO or SO samples concerns the overall redox state attained upon outgassing at T_v=773 K in each case. While the spectrum of the fresh sample shows methoxy species adsorbed on oxidised cations, those of samples MO or SO present features of species adsorbed on both oxidised and reduced cerium cations. Correlation with the EPR results (Fig. 1–3) suggests that while both cus-Ce^{4+} and cus-Ce^{3+} ions are formed upon outgassing at T_v=773 K in every case, the former largely predominate on the fresh sample, indicating the higher surface reducibility under vacuum (in the conditions used here) of the low surface area samples MO or SO. This correlates well with the larger linewidth (which may be due to a higher surface

concentration of paramagnetic species, leading to magnetic dipolar broadening) and also with the lower stability (when warming to RT) of the EPR signals due to superoxide species formed at 77 K on the latter samples (Fig. 3), as discussed above; attainment of comparable intensities of superoxide species when comparing the fresh with MO or SO samples, in spite of the signi ficant diff erence in s further correlation. On the other hand, the apparent red shift of the band due to on-top methoxy species adsorbed on Zr^{4+} which appears on the fresh sample (1153 cm^{-1}) in comparison to that observed over high surface pure zirconia (1163 cm^{-1})[8] can be attributed to the influence of nearby cerium cations, thus giving support to the above discussion on EPR results indicating that a mixed oxide surface structure is actually present on that sample.

Concerning the surface structure of MO and SO samples, and recalling the above discussion on EPR results, the fact that the infrared spectra of these sintered specimens (Fig. 4) present bands due to on-top methoxy species adsorbed on Zr^{4+} (less blue-shifted from the pure zirconia position than those observed in the fresh sample) indicates that the absence of O_2^--Zr^{4+} in the EPR spectrum of these samples (Fig. 2) must be interpreted rather as due to segregation of zirconia (or of a mixed oxide phase highly enriched in zirconium) in separate regions, forming at the surface of the samples islands which have little or no reducibility upon outgassing at T_v=773 K. Accordingly, the observation of O_2^--Ce^{4+} species with characteristics similar to those observed on pure ceria indicates that cerium appears at the surface as islands of ceria (or of a mixed oxide highly enriched in Ce). Anyway, some overall cerium enrichment at the surface seems also to be produced in the course of the thermal pretreatments undergone by these samples, since the intensity ratio (I_{Ce}/I_{Zr}) of on-top methoxy species adsorbed on cerium and zirconium cations is lower in the fresh sample than in the sintered specimens; note that such cerium-enrichment of surfaces with high temperature treatment is in line with results obtained by other research groups on similar samples.[23,24] Beyond this result, the low S/N ratio of the FTIR spectra obtained here for samples SO and MO, together with the complexity of this spectral region, make it di fficult to determine the nature of the adsorpti us from reaching more de finitive and between MO and SO samples in the FTIR spectra, we can tentatively correlate the detection in sample MO of a higher proportion of the type of O_2^--Ce^{4+} species related with associated vacancy centers (signal OC2, Fig. 2) with the higher amount of doubly bridging methoxy species detected in this specimen (Fig. 4). Further work is certainly required to clarify these points.

3.3. E ffects of pretreatment on the TPR profiles

The e ffects of pretreatment on the reduction profiles of $Ce_{0.5}Zr_{0.5}O_2$ mixed oxides are reported in Fig. 5. Fresh $Ce_{0.5}Zr_{0.5}O_2$ displays a single broad reduction feature centred at 850 K (trace a). This reduction pattern is consistent with previous observations indicating that TPR profiles of single phase CeO_2-ZrO_2 mixed oxides generally present a single reduction peak.[20] The comparison of trace a with the baseline

profile (non-horizontal due to buoyancy e ffects) inclu
broad H_2 adsorption resulting in a significant tailing at the high temperature end of the reduction peak. The baseline was not recovered until isothermal reduction at 1273 K was carried out. As checked by using a mass spectrometer as detector, some water evolution corresponds to this H_2 consumption. A possible explanation for this continuous water evolution/H_2 consumption is that, apart from the reduction of the mixed oxide, deep sintering of the sample occurs, which leads to a collapse of the surface area from the initial value of 40 $m^2 g^{-1}$ to ca. 2 $m^2 g^{-1}$ after the first TPR. Such a process may well interfere with the reduction process, accounting for the continuous evolution.

The TPR profile reported in trace b of Fig. 5, obtained on a sample which had been subjected only to a TPR run followed by MO treatment, just shows some displacement of the reduction peak to higher temperature compared to the fresh sample. This contrasts with a recent investigation of a $Ce_{0.68}Zr_{0.32}O_2$ mixed oxide, where it was observed that the pretreatment conditions critically a ffect the redox behaviour.[5] followed by a MO pretreatment shifted the reduction process to low temperatures (below 800 K), while a SO pretreatment reversibly shifted the reduction process above 800 K; such observation was consistent with a previous study of this laboratory on the redox behaviour of a $Ce_{0.5}Zr_{0.5}O_2$ mixed oxide[15] (it should be noted, however, that the $Ce_{0.5}Zr_{0.5}O_2$ mixed oxide used in this latter study contained about 8% of a CeO_2-rich minority phase, which could have a ffected the reduction behaviour;[25] on the contrary, no shift of the reduction peaks to low temperature was observed, even for three consecutive TPR/MO sequences (data not shown). The reversible redox behaviour was however observed also on the present $Ce_{0.5}Zr_{0.5}O_2$ mixed oxide when it was subjected to a SO/TPR/MO redox ageing (Fig. 5, trace d). After the sample was subjected to this kind of redox-ageing, the reduction process was split into two parts, most of the reduction occurring around 660 K while a minor peak remained at 900 K. A subsequent SO changed again the reduction profile, leading to a single reduction peak at 920 K; these changes were reversible, as evidenced by repeating alternately these treatments (Fig. 5(e)–(g)). It must be added that the presence of low temperature reduction processes as shown in traces d and f of Fig. 5 cannot be associated with incomplete desorption of water formed in the re-oxidation process, as this was checked separately by re-oxidising and adding some water at 700 K to a TPR/SO treated $Ce_{0.5}Zr_{0.5}O_2$.

To summarise, the following three types of H_2-reduction behaviour can be observed for $Ce_{0.5}Zr_{0.5}O_2$, provided that single phase product is analysed: (i) a single, relatively broad high temperature (HT) reduction feature centred at approximately 850 K, which is characteristic of a fresh sample; (ii) a similar reduction profile as above, but shifted to somewhat higher temperature, which is characteristic of samples having been subjected to a SO-type calcination immediately before the TPR experiment (irrespective of their earlier history) as well as of samples which from the fresh state have been subjected to repetitive TPR/MO sequences, but never to a SO; and (iii) a predominant reduction peak at a low temperature (around 660 K, LT) followed by some residual reduction occurring around 900–950 K, which is observed for any sample after a TPR/MO sequence provided that a SO-type treatment was applied in some previous moment. It may be added here that this latter

SO-type treatment requires that the sample handling at high temperature is carried out on an oxidised sample; i.e. a MO-type oxidation followed by heating at 1273 K under inert gas atmosphere generates the SO-species as well. It thus appears that a SO pretreatment, i.e. high temperature treatment of an oxidised sample, performed either initially or during the redox-ageing, followed by a TPR/MO sequence is an essential prerequisite to induce the low temperature reduction behaviour. Indeed, once the sample has experienced the SO pretreatment the reduction behaviour becomes extremely sensitive to the experimental sequence: when the TPR is followed by MO treatment an easily reducible state is generated, and conversely, when a SO treatment is applied, a solid is obtained which is reducible only at high temperatures. For the sake of clarity, in the text we indicate the species featuring the HT peak (case (ii) above) as SO pretreated, while the MO label designates a sample featuring the LT peak as it is generated from the SO sample by a TPR/MO treatment. Such MO and SO species easily and reversibly interconvert, as checked by alternating the TPR/MO and TPR/SO sequences at least 10 times. Notice that the present ‘‘reversible’’ redox behaviour is consistent with previous observations that also reported similar reversibility for samples of other compositions.[26] It is also worth recalling that in both cases the samples had been subjected to high temperature calcination before use. These observations were recently confirmed by a comparative study of a series of high and low surface area CeO_2-ZrO_2 mixed oxides, the latter being generated from high surface area samples by calcination at 1173 K. These studies showed that the favourable effects of the TPR sequence on the reduction behaviour are strongly improved by pre-sintering of the CeO_2-ZrO_2 mixed oxide.[27] However, such a high temperature oxidative pretreatment was not necessary to observe the promotional effect of the TPR when CeO_2-ZrO_2 mixed oxides containing CeO_2 impurities were investigated (*vide infra*).[15]

3.4. Isotopic studies of the effects of pretreatments on the reactivity

Hydrogen isotopic scrambling between the sample surface and gas phase hydrogen was detected during the TPR experiments by monitoring the m/z=3 signal (Fig. 6). Some signal at m/z=3 was always present in these traces, even in consecutive experiments carried out using $^2H_2$ as a reducing agent, due to the unavoidable presence of traces of water in the feeding lines, as already indicated in the Experimental section. Anyway, the comparison of these results with those in Fig. 5, where a comparable sequence of pretreatments was applied, indicates that irrespective of the applied pretreatment hydrogen scrambling occurs at a temperature which is significantly lower than that of the corresponding reduction peak/peaks. This suggests that, independent of the pretreatment conditions, H_2 is activated at the surface before any so-called irreversible reduction[28] (i.e. creation of oxygen vacancies) occurs. Even if one cannot discard the possibility that the activation of $^2H_2$ for such a scrambling process could be of a different type from (or even unrelated to) that required for the reduction process, the reversible shifts of the temperature of the peak maximum for the scrambling process with the pretreatments, i.e. with the presence of MO or SO species, suggest that a correlation between the two phenomena does exist, at least in terms of the ability of the surface to activate H_2. This is further reinforced by the fact that, as seen in Fig. 6, the scrambling behaviour of the species not subjected to the SO treatment is

different from the SO-treated sample since it features a peak at approximately 470 K, which disappears after the SO treatment.

If the same reduction scheme which has been proposed for CeO_2[29] (Scheme 1)* is considered also for $Ce_{0.5}Zr_{0.5}O_2$, then these results suggest that reaction (1) would not be a rate limiting step of the reduction process in any of the fresh, MO and SO states. To further elucidate the reduction mechanism of $Ce_{0.5}Zr_{0.5}O_2$ two series of experiments were carried out. First, a series of in situ TPR/TCD runs following the SO and MO pretreatments was carried out by using alternately $^1H_2$ and $^2H_2$ as reducing agent. This experiment was aimed at detecting isotopic effects on the

5. In fact the TPR profiles were

chosen.[30] An analogous experiment, previously reported for CeO_2, showed that the temperature of the TPR peak shifts reversibly by alternating $^1H_2$ and $^2H_2$ as reducing agent, evidencing the sensitivity of the TPR methodology to the isotopic effect. The TPR profiles obtained in these experiments (data not shown) were quite consistent with those reported in Fig. 5; the corresponding TPR peak temperatures are reported in Table 2. The examination of the peak temperatures for the reduction feature occurring around 660 K, which is observed after the MO pretreatment, shows a remarkable agreement between the values measured when both isotopes are employed in the reducing agent. In contrast, for both MO and SO pretreated samples there is a small but significant and reproducible isotope influence on the temperature of the peak maxima observed around 900 K. In both cases, when $^1H_2$ is employed as reducing agent the maximum reduction rate is observed at a lower temperature (7-12 K) than when using $^2H_2$. Notice that all these experiments were performed in situ on the same sample, to avoid experimental artifacts.

A second series of experiments was then carried out, varying the heating rate used in the TPR experiment. Monti and Baiker[30] showed that by plotting $\ln(c_M T_M^2/\beta)$ versus $1/T$, where c_M, T_M and β are respectively H_2 concentration, temperature at peak maximum and heating rate, an apparent activation energy for the reduction process can be obtained. An example of the Arrhenius plots thus obtained is shown in Fig. 7, and the resulting apparent activation energies are given in Table 2. The insensitivity of the LT peak to the isotopic effect is confirmed by the apparent activation energies of about 40 kJ mol^{-1} measured in both cases, which are equal within experimental error. For comparison, it may be recalled that apparent activation energies of about 50 kJ mol^{-1} were reported for CO oxidation over NM/CeO_2 catalysts under conditions where oxygen migration from the support is believed to be rate limiting.[31] In contrast, for the HT peak a much higher E_a is observed, which increases by about 25-35 kJ mol^{-1} when $^2H_2$ is employed as reducing agent instead of $^1H_2$.

These data strongly suggest that the rate determining step (RDS) of the reduction reaction is essentially different for the processes taking place within the LT

* The reaction mechanism shown in Scheme 1 follows that reported in ref. 29, however, it should be noted that the removal of water in the dehydroxylation of oxide surfaces (both in reductions and in other processes) is considered to be initiated by transfer of a proton from an OH group (more or less acidic) to another OH (more or less basic) to form cation-coordinated (adsorbed) H_2O, this latter subsequently desorbing from the cation(s) into the gas phase, rather than a single step process.

detected for the HT peak implies that the rate determining step in the latter includes forming and/or breaking of some bond(s) with hydrogen. As shown above, activation of the H_2 molecule (step 1 in Scheme 1) occurs at temperatures clearly lower than those of the irreversible reduction; therefore this is unlikely to be the RDS. Rather, the rate limiting step for the reduction process above 700 K could be the formation of adsorbed water molecules, or also their desorption. The first alternative seems much more likely, in view of the large values of both the activation energy and its isotopic effect. In contrast, the reduction process occurring below 700 K, together with the relative similarity between the corresponding activation energy and that of ceria reduction by CO discussed above, is a strong indication that in this case the reduction process is limited by the rate of oxygen diffusion from the bulk of the solid. This is consistent with $^{18}O/CO/O_2$ experiments carried out over CeO_2–ZrO_2 which suggested the importance of bulk migration at low reaction temperatures.[32]

To corroborate these hypotheses, in situ TPR/MS experiments were carried out using both $^1H_2$ and $^2H_2$ as reducing agents; profiles of hydrogen consumption and water production were thus obtained during reduction of SO and MO pretreated samples. Despite the different experimental conditions between TPR/MS and TPR/TCD, which could affect the TPR profiles,[33] good agreement between the two techniques was achieved. Fig. 8 presents these data for the $^2H_2$ case (together with the evolution of the m/z=3 signal, which reflects hydrogen scrambling); the water evolution curves obtained with the two isotopes for both samples are presented in Fig. 9, and the temperatures of the peak maxima are summarised in Table 3. The patterns found for both MO and SO species indeed appear fairly consistent with those reported in Fig. 5, although there is now a shoulder at about 500-520 K preceding the main LT reduction peak in the MO pretreated sample, which can be noticed both as hydrogen consumption and water evolution, especially when using $^2H_2$. This was not observed in the results of Fig. 5; there is no clear attribution of this difference, and it is probably due to the higher amount of the sample which had to be used in the TPR/MS experiment, some perturbation of the TPR profiles could occur, particularly at low temperatures where water desorption or accumulation in transfer lines could interfere in the reduction process.

In any case, the water evolution curves shown here reflect the same result given by the TPD/TCD experiments, i.e. that the temperature of the maximum reduction rate is affected by the isotope only for the HT reduction process, while the LT reduction is unaffected. Despite the molecular weight between deuterated and nondeuterated water, the reduction peak at 900 K is significantly affected by the change in the isotope, while the difference is not detected by the sample, except for the above-mentioned shoulder at 500 K (Fig. 9). In both peaks there is a visible shift between the temperatures of the maxima for hydrogen consumption and water desorption (15-20 K for the MO peak and 45-48 K for the SO sample), which is in agreement with the reduction scheme reported above, i.e. that the reduction process occurs via initial hydrogen activation (reversible reduction) followed by a slower water formation/desorption (irreversible reduction),[34] although some contribution of experimental artifacts to this delay in water evolution cannot be excluded. In summary, these experiments suggest that

under our experimental conditions water formation presumably limits the reduction rate in the process observed at high temperatures. Consistently, desorption of physically adsorbed water was completed by about 500 K, as observed in the initial cleaning pretreatment.[11]

3.5. Relationship between bulk diffusion and reduction rates

An estimation of the rate (or of any other related quantity) at which oxygen migrates from the bulk of the mixed oxide to the surface can be made and used to check the consistency of the reduction model given above. For such a calculation the bulk oxygen diffusion coefficient is r
measurements of D_O for a $Ce_{0.5}Zr_{0.5}O_2$ mixed oxide. Values for it can, in principle, be calculated from electrical conductivity and transfer numbers data using the following expression:

$$D_o = \frac{H_F \sigma_i k T}{C_i (Ze)^2}$$

where D_O (cm^2 s^{-1}) is the diffusion coefficient, σ_i (Ω^{-1} cm^{-1}) the ionic conductivity, k the Boltzmann constant (J K^{-1}), H_F is the Haven ratio (0.78146 for a f.c.c. structure), T the temperature (K), C_i the concentration of charge carriers ((O atoms) cm^{-3}) and Ze their charge (C). Such electrical property data have been reported by Chiodelli et al.[35] for ceria–zirconia materials with several Ce:Zr ratios, prepared by ceramic methods; these solids calcined at high temperature should, in principle, be considered comparable to our SO samples. The values of D_O calculated in this way are higher that those previously reported for CeO_2: for example, for our Ce:Zr ratio we obtain D_O=2x10^{-13} cm^2 s^{-1} at 723 K, which is significantly higher than the values of 2x10^{-20} and 5x10^{-18} cm^2 s^{-1} reported respectively in ref. 36 and 37 for pure ceria. This is however consistent with recent studies of oxygen mobility in the bulk of CeO_2-ZrO_2 mixed oxides by Madier et al., who showed that Ce^{4+}/Zr^{4+} isomorphous substitution enhances the exchange of oxygen in the bulk.[38]

The relevance of the diffusion to th
diffusion length (in the crystallites),
(1 s) is determined (from the D_O values) as a function of temperature (Fig. 10). Note that a discontinuity appears in this figure due to a change in activation energy and pre-exponential factor observed by Chiodelli et al.[35] The mean diffusion path $Ce_{0.5}Zr_{0.5}O_2$ materials computed equa
around 700 K, which is of the same order of magnitude as the temperature at which the maximum of the reduction rate (LT peak) occurs in the MO treated sample. In principle, these diffusion leng
computed from Chiodelli's data, are applicable to SO-type samples, but as an initial approximation we may take them as valid also for MO treated ones (more on this below). This result is thus already a first indication agreeing with the idea that in this latter material the overall solid reduction is achieved when diffusion allo
the oxygen ions to travel from the bulk to the surface, even though the occurrence of grain boundary effects at high temperatures cannot be excluded.[35] It is also compatible with a surface related rate determining step in

the case of SO samples, since at the temperature at which reduction of these is seen to occur, the anion diffusion in the bulk is much faster and does not limit the p

To make the analysis more exact, one must take into account that in the TPR experiments oxygen atom migration occurs under an oxygen concentration gradient, due to the fact that the reduction proceeds from the surface to the bulk. Indeed, in the reduction occurring in MO samples within the LT peak, which is the one being discussed now, the surface reduction is presumed to occur (and be completed) faster than that of the bulk, as suggested by the joint consideration of the hydrogen scrambling experiments reported above (which concern the activation of hydrogen) and of the lack of isotopic effect in this implies that the formation of water, and consequently of surface anion vacancies, is not rate determining). Thus one may assume, as a first approximation, that the external surface is completely reduced during this LT reduction, i.e. at the surface region the oxygen ion concentration would be 87.5% of the maximum. Upon application of Fick's law of diffusion, the oxygen flux N (molecules cm^{-2} s^{-1}) can be calculated:

$$N = \frac{D_0(c_b - c_s)}{r}$$

where c_b and c_s represent the concentration of oxygen atoms in the particle center (5.38×10^{22} (O atoms) cm^{-3}) and at the surface layer (4.71×10^{22} (O atoms) cm^{-3}); r (6.5×10^{-7} cm) is the length of the diffusion, the radius of the particles. Using these values a rate of oxygen migration to the surface can be calculated as a function of temperature and compared with the experimental rate of H_2 consumption expressed as the rate of release of oxygen atoms (Fig. 11). As expected the oxygen flux increases steeply with the temperature. It is particularly interesting to observe that, even under the highest gradient possible, i.e. fully reduced surface and fully oxidised bulk (curve x=2 in Fig. 11), the experimental rate observed at the beginning of the reduction process is much higher than the calculated flux. For the sake of comparison, Fig. 11 reports some additional curves (lower x values) which represent intermediate degrees of reduction of the bulk; qualitative analysis reveals differences wh model used. This might indicate that the diffusion coefficient in the MO is higher than that of the SO-type solids (as in the work by Chiodelli et al.); however, this conclusion is not firm since D_O can change when varying the amount of oxygen vacancies in the bulk.[39] Finally, it is important to note that the rate of diffusion of the oxygen atoms to the surface d surface area, the lower r and consequently the higher the flux. This could easily contribute to the sensitivity of the reduction behaviour of the CeO_2-ZrO_2 mixed oxides to the textural properties.

3.6. Implications of the data for models of ceria–zirconia reduction

Two main points arise from the preceding results and discussions. First, the important and reversible modification in redox behaviour observed when cycling between MO and SO states requires in these samples a previous SO-type high temperature oxidation. The spectroscopic measurements suggest that the modification induced by this treatment may have, as a key aspect, a change in surface structure in which pure ceria-like

islands appear (the possible simultaneous existence of some pure zirconia-like islands being not detrimental in this); the fact that, in other studies using samples which contained a CeO_2 impurity, such previous SO treatment was not necessary to obtain the reversible behaviour agrees with this.

Secondly, the question arises: what is the reason for this reversible e ffect? The T isotopic e ffects inclu some step involving breaking or formation of O–H bonds, is di fficult and c of the bulk by H_2, which consequently only occurs at temperatures around 900 K; but in MO samples the reduction of the surface is made much easier, to such an extent that it can occur at temperatures below 550 K. A consequence is that the overall reduction rate becomes limited by the oxygen di ffusion in th begins to be fast enough around 600–700 K. It must be noted here that, within this scheme, the data reported in this work do not clarify whether in SO-type samples the oxygen di ffusion rate that in MO-type samples, although the study summarised in Fig. 11 suggests that such di ffusion coul somewhat faster in the latter. The reason for this large change in surface behaviour, however, remains unclear. The spectroscopic data do not show large changes in surface composition, although rearrangements of the surface cations in their mutual lateral disposition might occur, as hinted by the FTIR spectra. The di fferences in surface structure would thus be of some subtle nature. Certainly the EPR data would imply that the reducibility by vacuum treatments is not very di fferent in th the latter would be more reducible, in apparent contradiction with the TPR results—but these latter use H_2 as reducing agent, which is a di fferent story reaction steps involving O–H bonds.

Although the situation remains still unresolved in this respect, it is worth noting that there might be some connection between the redox behaviour observed here and the results of neutron di ffraction stu by Mamontov et al.[40] These authors detected, in reoxidised ceria-zirconia materials, oxygen atoms located in rather substantial amounts in interstitial positions of the structure (in octahedral interstices of the f.c.c. cation lattice), while part of the normal anion sites (the tetrahedral ones) remained unoccupied. The same observation was reported also by Thomson et al.[41] Such interstitial oxygens accompanied by vacancies in the regular lattice sites (i.e. Frenkel defects) could be detected also by Mamontov et al.[40] in pure ceria; in this latter oxide the interstitials disappeared, filling the regular sites, upon calcination above ca. 900 K, but for their ceria–zirconia material (having atomic ratio Ce:Zr=2:1) their amount remained unchanged after treatment up to 1050 K (the highest temperature used there). Those authors pointed out that this interstitial oxygen species could be more mobile and easily removable than the regular lattice ones, so that they could be responsible for the good oxygen bu ffering properties of ceria. To hypothesise that such interstitials could be present in our MO treated specimens but be absent in SO-type samples due to their recombination with the anion lattice site vacancies upon calcination at some temperature in the 1050–1250 K range (in a similar way as shown to occur in ref. 40 for pure ceria at lower temperatures); and that these interstitials could then be responsible for the LT peak detected in TPR experiments on the MO samples. Of course, if this were

so, among those interstitial species only those present at the surface would play an important role, since the main large di fference bet di fferent ease have a basicity signi ficantly diff kinetics of the water formation steps. The verification of such a hypothesis would require other types of experiments, able to discriminate the properties of any such unusual anion species at the surface.

4. Conclusions

The present work confirms that the reduction behaviour of $Ce_{0.5}Zr_{0.5}O_2$ solid solution is strongly a ffected by pretreatments. A relatively stable, single-peak reduction profile can be observed on a high surface area, single-phase product of this stoichiometry. A high temperature oxidative treatment, leading to strong sintering, is necessary to modify this behaviour, generating a system whose reduction behaviour becomes highly sensitive to the pretreatment. As revealed by the spectroscopic study of O_2 and methanol adsorption, the surface structure and reactivity are strongly modified by such oxidative pretreatment: pure ceria-like surface islands appear and higher amounts of surface oxygen vacancies are generated by vacuum treatment which are more easily reoxidised than on the initial fresh sample. However, according to these techniques the thermal cycling treatments which modify strongly and reversibly the redox ability of the high temperature preoxidised material do not lead to large structural changes at the surface. Use of $^1H_2$ and $^2H_2$ as reducing agent under the TPR conditions has allowed us to elucidate important features of the reduction mechanism of these CeO_2-ZrO_2 mixed oxides. It appears that the low-temperature reduction behaviour of the CeO_2-ZrO_2 mixed oxides observed in samples reoxidised at low temperature have their rate controlled by the properties of the bulk of the oxide, the surface processes being faster in comparison. In contrast, the reduction features occurring at higher temperatures (the only ones present in samples reoxidised at high temperature) are controlled by surface processes, possibly related to water evolution, which are now slower than anion di ffusion in bulk.

Acknowledgements

Helpful discussions with Prof. Alessandro Trovarelli (University of Udine), Dr. Gabriele Balducci and Dr. Roberta Di Monte (University of Trieste) are gratefully acknowledged. Dr. Roberta Di Monte is also acknowledged for the XRD measurements. CICYT (project Nr. MAT2000-1467), University of Trieste, CNR (Roma) Programmi Finalizzati ‘‘Materiali Speciali per Tecnologie Avanzate II, Contract n. 97.00896.34 and ‘‘Regione Friuli Venezia-Giulia, Fondo regionale per la ricerca’’ are gratefully acknowledged for financial support. A. B. H. and A. M.-A. wish to thank the Comunidad de Madrid for grants under which this work has been carried out.

References

1 J. Kašpar, M. Graziani and P. Fornasiero, in Handbook on the Physics and Chemistry of Rare Earths: The Role of Rare Earths in Catalysis, ed. K. A. Gschneidner, Jr. and L. Eyring, Elsevier, Amsterdam, 2000, ch. 184, pp. 159–267.

2 C. E. Hori, H. Permana, K. Y. S. Ng, A. Brenner, K. More, K. M. Rahmoeller and D. N. Belton, Appl. Catal. B, 1998, 16, 105.

3 P. Fornasiero, R. Di Monte, G. Ranga Rao, J. Kašpar, S. Meriani, A. Trovarelli and M. Graziani, J. Catal., 1995, 151, 168.

4 G. Balducci, P. Fornasiero, R. Di Monte, J. Kašpar, S. Meriani and M. Graziani, Catal. L ett., 1995, 33, 193.

5 R. T. Baker, S. Bernal, G. Blanco, A. M. Cordon, J. M. Pintado, J. M. Rodriguez-Izquierdo, F. Fally and V. Perrichon, Chem. Commun., 1999, 149.

6 N. Hickey, P. Fornasiero, J. Kašpar, M. Graziani, G. Blanco and S. Bernal, Chem. Commun., 2000, 357.

7 A. Martínez-Arias, M. Fernández-Garcia, C. Belver, J. C. Conesa and J. Soria, Catal. Lett., 2000, 65, 197.

8 G. Colón, M. Pijolat, F. Valdivieso, H. Vidal, J. Kašpar, E. Finocchio, M. Daturi, C. Binet, J. C. Lavalley, R. T. Baker and S. Bernal, J. Chem. Soc., Faraday Trans., 1998, 94, 3717.

9 P. Fornasiero, J. Kašpar and M. Graziani, Appl. Catal. B, 1999, 22, L11.

10 P. Vidmar, P. Fornasiero, J. Kašpar, G. Gubitosa and M. Graziani, J. Catal., 1997, 171, 160.

11 M. Daturi, C. Binet, J. C. Lavalley, H. Vidal, J. Kašpar, M. Graziani and G. Blanchard, J. Chim. Phys., 1998, 95, 2048.

12 P. Fornasiero, R. Di Monte, J. Kašpar, T. Montini and M. Graziani, Stud. Surf. Sci. Catal., 2000, 130, 1355.

13 M. Yashima, H. Arashi, M. Kakihana and M. Yoshimura, J. Am. Ceram. Soc., 1994, 77, 1067.

14 G. W. Graham, W. H. Weber, C. R. Peters and R. K. Usmen, J. Catal., 1991, 130, 310.

15 P. Fornasiero, G. Balducci, R. Di Monte, J. Kašpar, V. Sergo, G. Gubitosa, A. Ferrero and M. Graziani, J. Catal., 1996, 164, 173.

16 J. Soria, A. Martínez-Arias and J. C. Conesa, J. Chem. Soc., Faraday Trans., 1995, 91, 1669

17 A. Martínez-Arias, J. Soria, J. C. Conesa, X. L. Seoane, A. Arcoya and R. Cataluña, J. Chem. Soc., Faraday Trans., 1995, 91, 1679.

18 H. Nöremberg and G. A. D. Briggs, Phys. Rev. Lett., 1997, 79, 4222.

19 M. Anpo, M. Che, B. Fubini, E. Garrone, E. Giamello and M. C. Paganini, Top. Catal., 1999, 8, 189.

20 J. Kašpar, P. Fornasiero and M. Graziani, Catal.Today, 1999, 50, 285.

21 F. Fally, V. Perrichon, H. Vidal, J. Kašpar, G. Blanco, J. M. Pintado, S. Bernal, G. Colon, M. Daturi and J. C. Lavalley, Catal. Today, 2000, 59, 373.

22 M. Daturi, E. Finocchio, C. Binet, J. C. Lavalley, F. Fally, V. Perrichon, H. Vidal, N. Hickey and J. Kašpar, J. Phys. Chem. B, 2000, 104, 9186.

23 V. Sergo and D. R. Clarke, J. Am. Ceram. Soc., 1995, 78, 641.

24 G. W. Graham, C. L. Roe, L. P. Haack and A. M. Straccia, J. Vac. Sci. Technol. A, 2000, 18, 1093.

25 T. Egami, W. Dmowski and R. Brezny, Soc. Automot. Eng., [Spec. Publ.] SP, 970461, 1997.

26 S. Otsuka-Yao-Matsuo, T. Omata, N. Izu and H. Kishimoto, J. Solid. State. Chem., 1998, 138, 47.

27 H. Vidal, J. Kašpar, M. Pijolat, G. Colón, S. Bernal, A. M. Cordon, V. Perrichon and F. Fally, Appl. Catal. B, 2000, 27, 49.

28 S. Bernal, J. J. Calvino, G. A. Cifredo, J. M. Rodríguez-Izquierdo, V. Perrichon and A. Laachir, J. Catal., 1992, 137, 1.

29 J. El Fallah, S. Boujana, H. Dexpert, A. Kiennemann, J. Majerus, O. Touret, F. Villain and F. Le Normand, J. Phys. Chem., 1994, 98, 5522.

30 D. A. M. Monti and A. Baiker, J. Catal., 1983, 83, 323.

31 T. Bunluesin, E. S. Putna and R. J. Gorte, Catal. Lett., 1996, 41, 1.

32 M. Boaro, C. de Leitenburg, G. Dolcetti and A. Trovarelli, J. Catal., 2000, 193, 338.

33 G. Fierro, M. LoJacono, M. Inversi, P. Porta, R. Lavecchia and F. Cioci, J. Catal., 1994, 148, 709.

34 S. Bernal, J. J. Calvino, G. A. Cifredo, J. M. Gatica, J. A. Pérez Omil and J. M. Pintado, J. Chem. Soc., Faraday Trans., 1993, 89, 3499.

35 G. Chiodelli, G. Flor and M. Scagliotti, Solid State Ionics, 1996, 91, 109.

36 M. Kamiya, E. Shimada and Y. Ikuma, J. Ceramic. Soc. Jpn., 1998, 106, 1023.

37 D. Martin and D. Duprez, J. Phys. Chem., 1996, 100, 9429.

38 Y. Madier, C. Descorme, A. M. LeGovic and D. Duprez, J. Phys. Chem. B, 1999, 103, 10999.

39 B. C. H. Steele and J. M. Floyd, Proc. Br. Ceram. Soc., 1971, 72, 55.

40 E. Mamontov, T. Egami, R. Brezny, M. Koranne and S. Tyagi, J. Phys. Chem. B, 2000, 104, 11110.

41 J. B. Thomson, A. R. Amstrong and P. G. Bruce, J. Solid State Chem., 1999, 148, 56.

Table 1. Spectral characteristics and assignments of the EPR signals obtained upon oxygen adsorption on outgassed $Ce_{0.5}Zr_{0.5}O_2$ samples.

Signal	EPR parameters[a]	Assignment
OC1	$g_{\parallel} = 2.034$, $g_{\perp} = 2.011$	O_2^--Ce^{4+} formed on isolated oxygen vacancies
OC1'	$g_z = 2.031$, $g_x = 2.017$, $g_y = 2.011$	
OC2	$g_{\parallel} = 2.047$-2.041, $g_{\perp} \approx 2.010$	O_2^--Ce^{4+} formed on associated oxygen vacancies
OZ	$g_z = 2.034$, $g_y = 2.009$, $g_x = 2.002$	O_2^--Zr^{4+}

[a] Axes attribution in the g-tensor follows criteria of previous works [16].

Table 2. Temperatures of the maximum reduction rate in the TPR/TCD profiles, apparent activation energies and oxygen uptake at 700 K measured after the TPR experiment obtained on the $Ce_{0.5}Zr_{0.5}O_2$.

Pre-treatment	Technique	Temperature of peak maxima (K) and Activation Energy (kJ mol^{-1})[a]				O_2 uptake (ml g^{-1})[a]
		LT		HT		
		T_m	E_a	T_m	E_a	
Fresh	TPR/$^1H_2$			850		
SO		-	-	914	90	17.5
MO		659	39	896	91	17.4
MO		663		896		17.6
SO	TPR/$^2H_2$	-	-	921	134	17.4
MO		659	44	908	116	17.3
MO		664		908		17.6

[a] Standard deviations: Activation energy ± 3.5 kJ mol^{-1}; O_2 uptake 0.2 ml g^{-1}.

Table 3. Temperatures of the maximum reduction rate in the TPR/MS profiles obtained on the $Ce_{0.5}Zr_{0.5}O_2$ subjected to severe (SO) and mild (MO) pre-oxidation.

Pre-treatment	m/e[a]	Temperature of peak maxima (K)			
		TPR / $^1H_2$ - MS		TPR / $^2H_2$ - MS	
SO	2 or 4	913		925	
	18	961		971	
	19	961		970	
	20	-		969	
MO	2 or 4	660	895	660	910
	18	678	910	675	938
	19	679	910	676	940
	20	-	-	678	940

[a] As described in the experimental section due to presence of traces of water, m/e=19, i.e. partially deuterated product was also detected.

Scheme 1

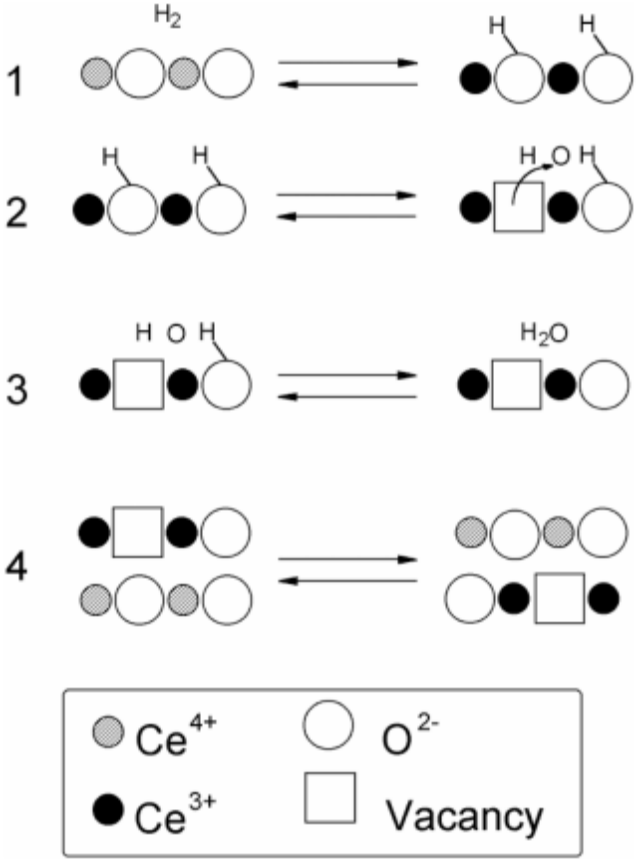

Captions for Figs.

Fig. 1 EPR spectra of the $Ce_{0.5}Zr_{0.5}O_2$ specimens: (a) fresh sample after O_2 adsorption at 77 K, warming to RT for 12 h and outgassing at RT. EPR spectra of sample MO: (b) outgassed at T_v=773 K; (c) subsequent O_2 adsorption at 77 K; (d) subsequent warming for 1 min to RT. (e)–(g) The same as (b)–(d) for sample SO.

Fig. 2 Experimental EPR spectra and computer simulation (individual components and total) of the spectra observed after O_2 adsorption at 77 K on the indicated samples outgassed at T_v=773 K.

Fig. 3 Evolution of the overall EPR integrated intensity of superoxide species in the O_2 adsorption experiments performed on samples SO and MO; w.t. refers to warming time when warming to RT.

Fig. 4 FTIR spectra following methanol adsorption at RT and outgassing at 373 K on the samples outgassed at T_v=773 K. (a) Fresh sample; (b) MO; (c) SO.

Fig. 5 Effects of pretreatments on in situ temperature programmed reduction profiles (TPR/TCD) obtained for $Ce_{0.5}Zr_{0.5}O_2$. Pretreatments: (a) fresh, (b) MO, (c) SO, (d) MO, (e) SO, (f) MO, (g) SO. Instrumental baseline is added under each trace.

Fig. 6 Effects of pretreatments on hydrogen scrambling (m/z=3) during in situ temperature programmed reduction profiles (TPR/MS) obtained for $Ce_{0.5}Zr_{0.5}O_2$. Pretreatments: (a) fresh, (b) MO, (c) MO, (d) SO, (e) MO, (f) SO, (g) MO.

Fig. 7 Arrhenius plot ($\ln(c_M T^2_M/\beta)$ versus 1/T) for the (a) HT and (b) LT peaks in the TPR profiles of $Ce_{0.5}Zr_{0.5}O_2$ subjected to a MO pretreatment. ($^1H_2$-TPR/TCD: filled symbols, $^2H_2$-TPR/TCD: open symbols).

Fig. 8 $^2H_2$-TPR/MS profiles for the SO (1) and MO (2) pretreated $Ce_{0.5}Zr_{0.5}O_2$.

Fig. 9 Comparison of evolution of m/z=18 in the $^2H_2$ (a) and $^1H_2$ (b) TPR/MS profiles obtained on the SO (1) and MO (2) pretreated $Ce_{0.5}Zr_{0.5}O_2$.

Fig. 10 Diffusion length (l) versus temperature. Values calculated from the data reported in ref. 35 using the equation $l = \sqrt{(2D_o t)}$ (diffusion time 1 s).

Fig. 11 Comparison of experimental reduction rate measured on $Ce_{0.5}Zr_{0.5}O_2$ subjected to the SO/TPR/MO pretreatment with the calculated oxygen flux to the surface (2 m^2 g^{-1}); x represents the degree of reduction in the bulk of $Ce_{0.5}Zr_{0.5}O_x$

Fig. 1

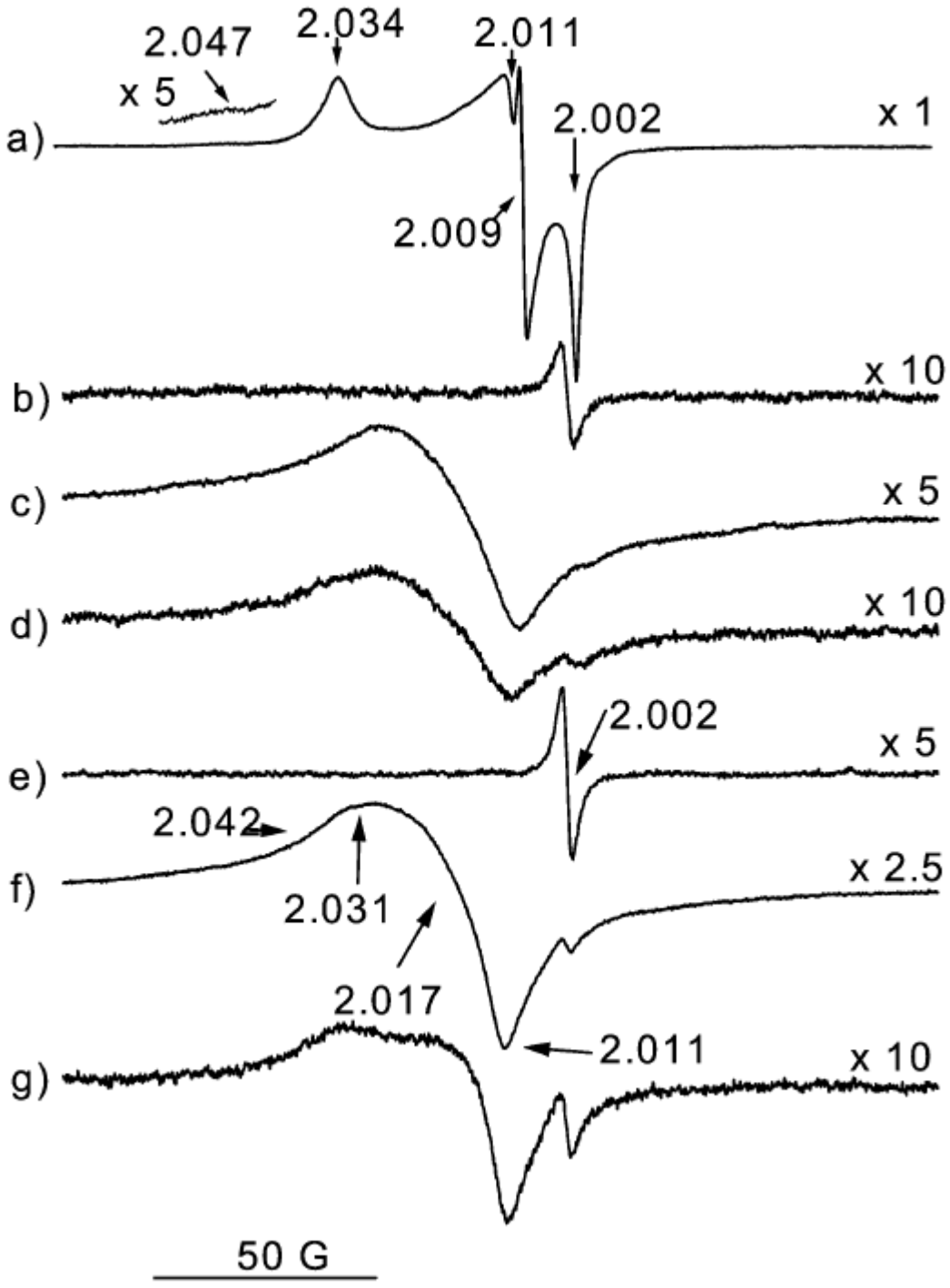
2.047
2.034
2.011
x 5
2.002
x 1
a)
2.009
x 10
b)
c)
x 5
d)
x 10
2.002
e)
x 5
2.042
f)
2.031
x 2.5
2.017
2.011
g)
x 10
50 G

Fig 2

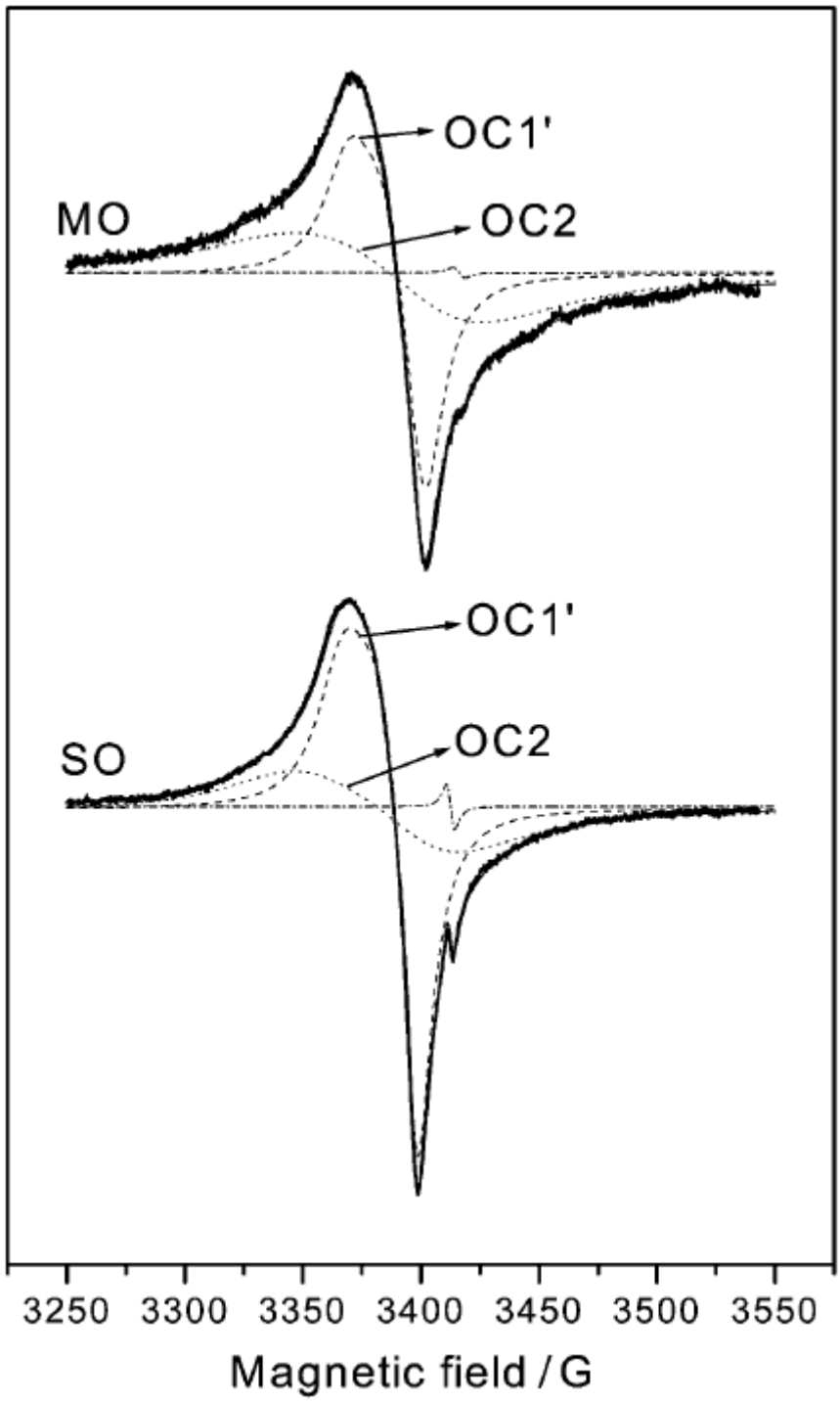
OC1'
MO
OC2
OC1'
SO
OC2
3250
3300
3350
3400
3450
3500
3550
Magnetic field / G

Fig. 3

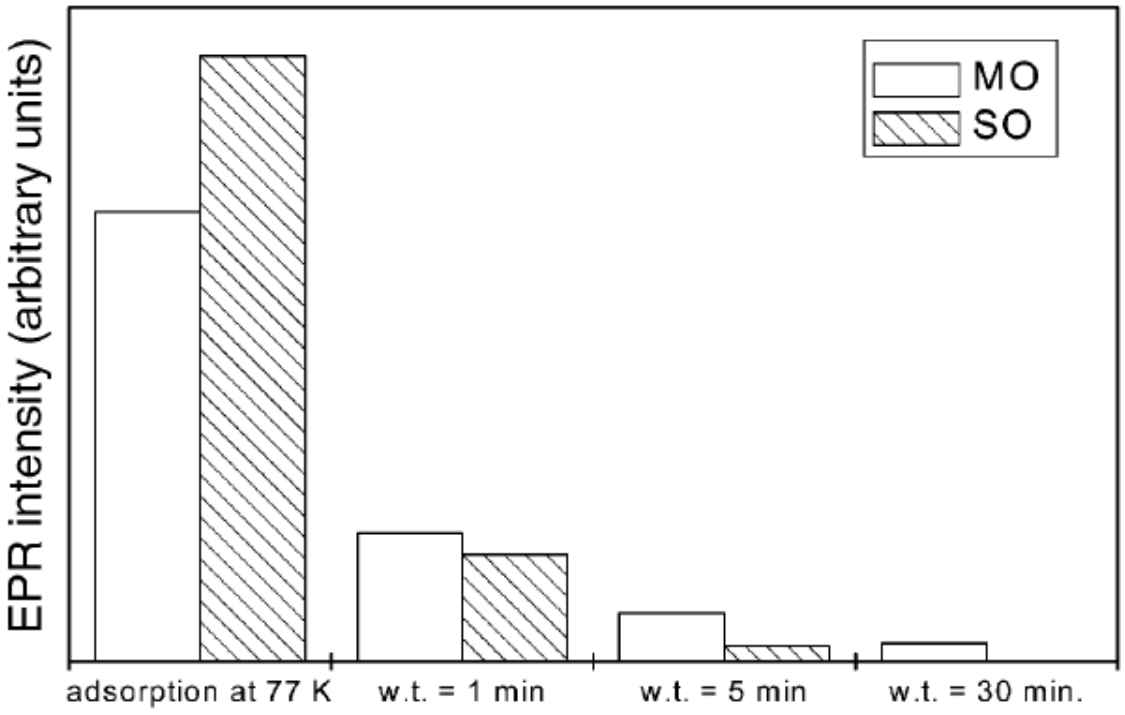
EPR intensity (arbitrary units)
MO
SO
adsorption at 77 K
w.t. = 1 min
w.t. = 5 min
w.t. = 30 min.

Fig. 4

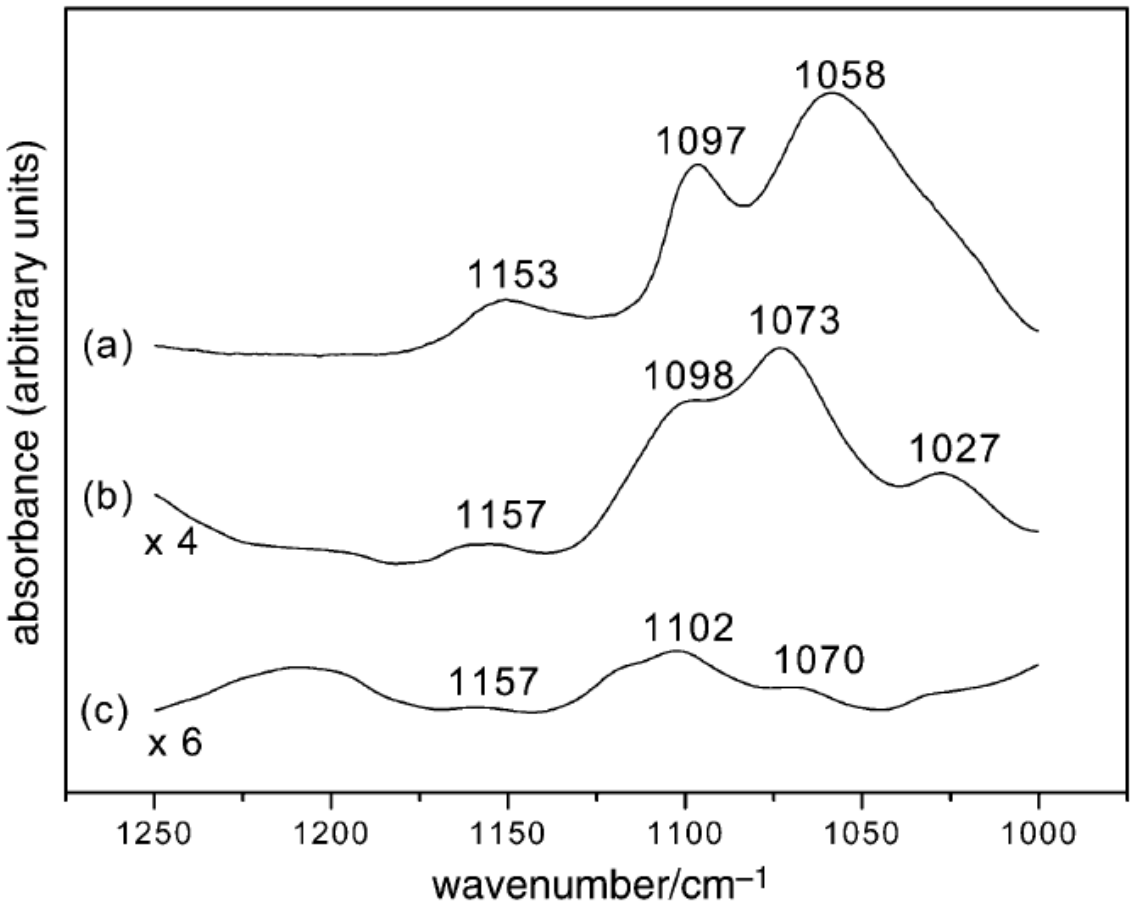
absorbance (arbitrary units)
1058
1097
1153
(a)
1073
1098
1027
(b)
x 4
1157
1102
1070
1157
(c)
x 6
1250
1200
1150
1100
1050
1000
wavenumber/cm⁻¹

Fig. 5

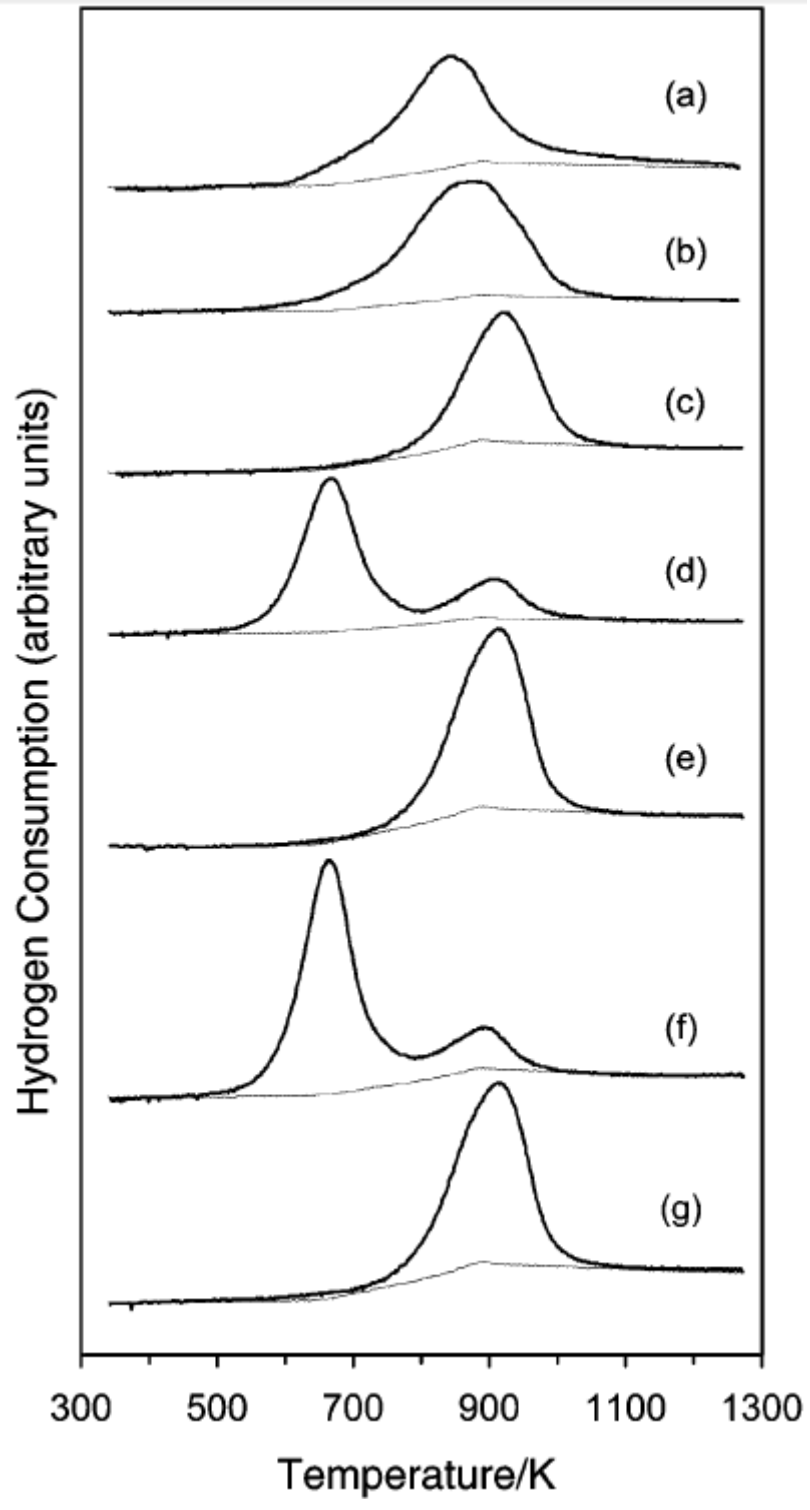
(a)
(b)
(c)
(d)
(e)
(f)
(g)
Hydrogen Consumption (arbitrary units)
300
500
700
900
1100
1300
Temperature/K

Fig. 6

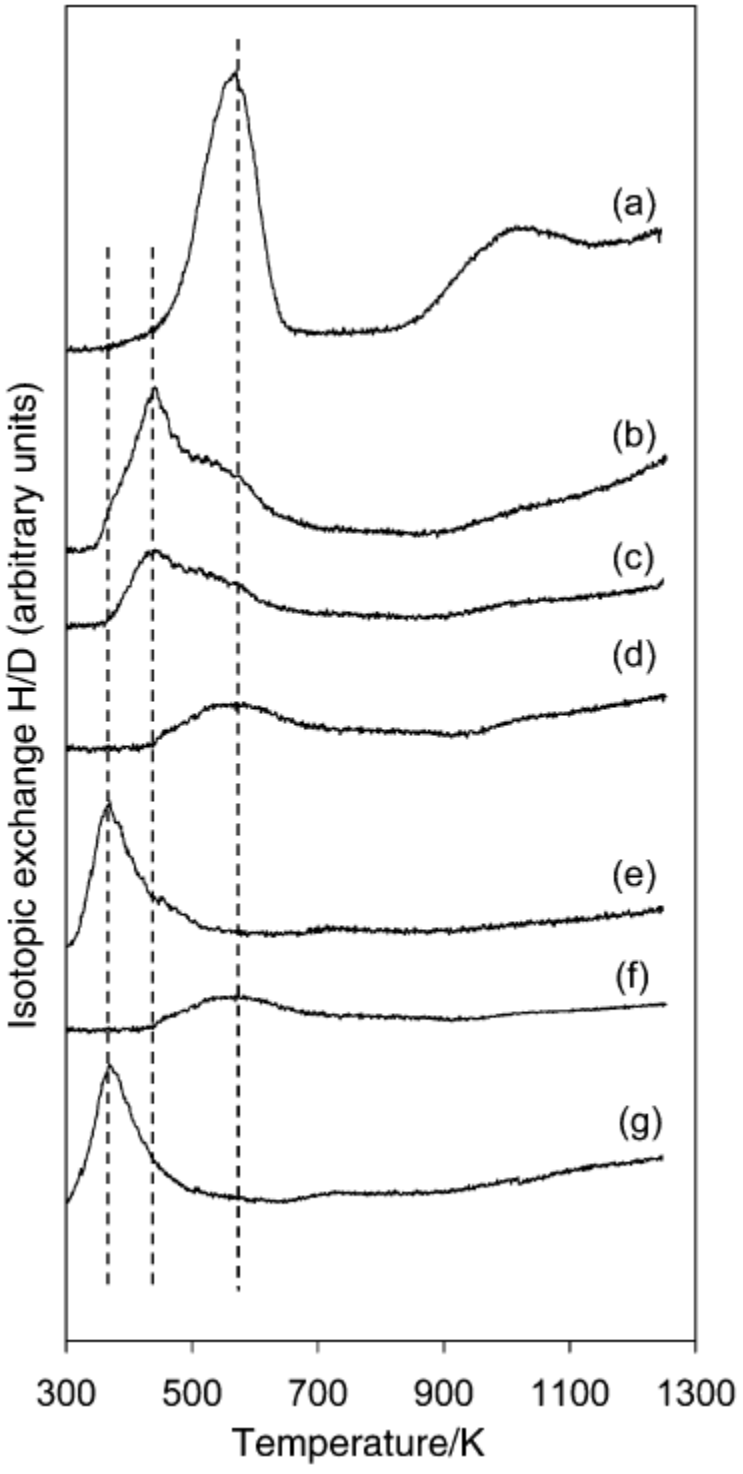
Isotopic exchange H/D (arbitrary units)
(a)
(b)
(c)
(d)
(e)
(f)
(g)
300
500
700
900
1100
1300
Temperature/K

Fig. 7

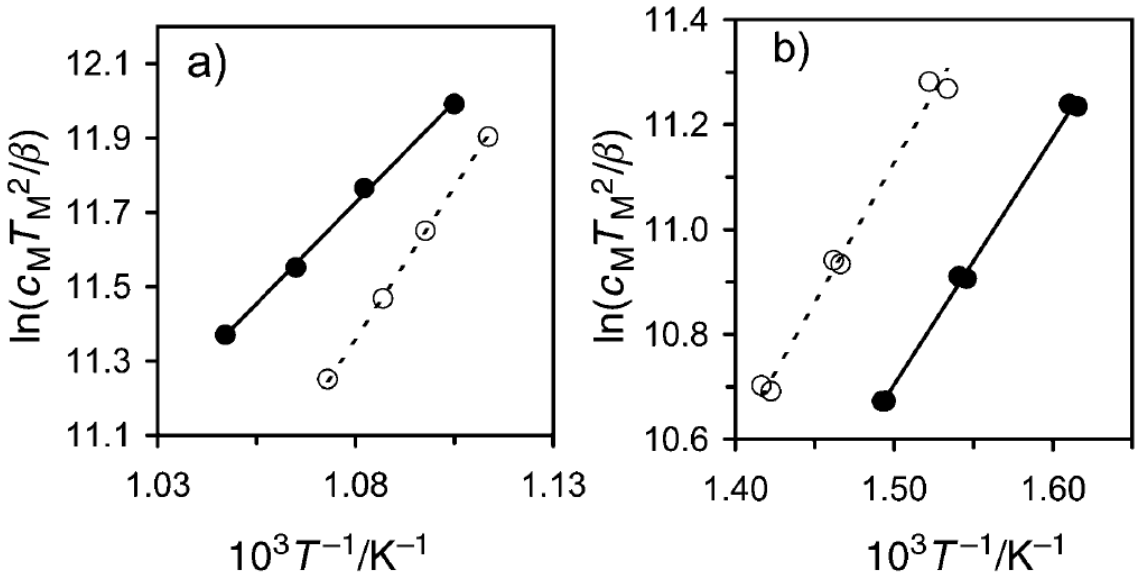
a)
b)
12.1
11.9
11.7
11.5
11.3
11.1
11.4
11.2
11.0
10.8
10.6
1.03
1.08
1.13
1.40
1.50
1.60
$\ln(c_M T_M^2/\beta)$
$10^3 T^{-1}/K^{-1}$

Fig. 8

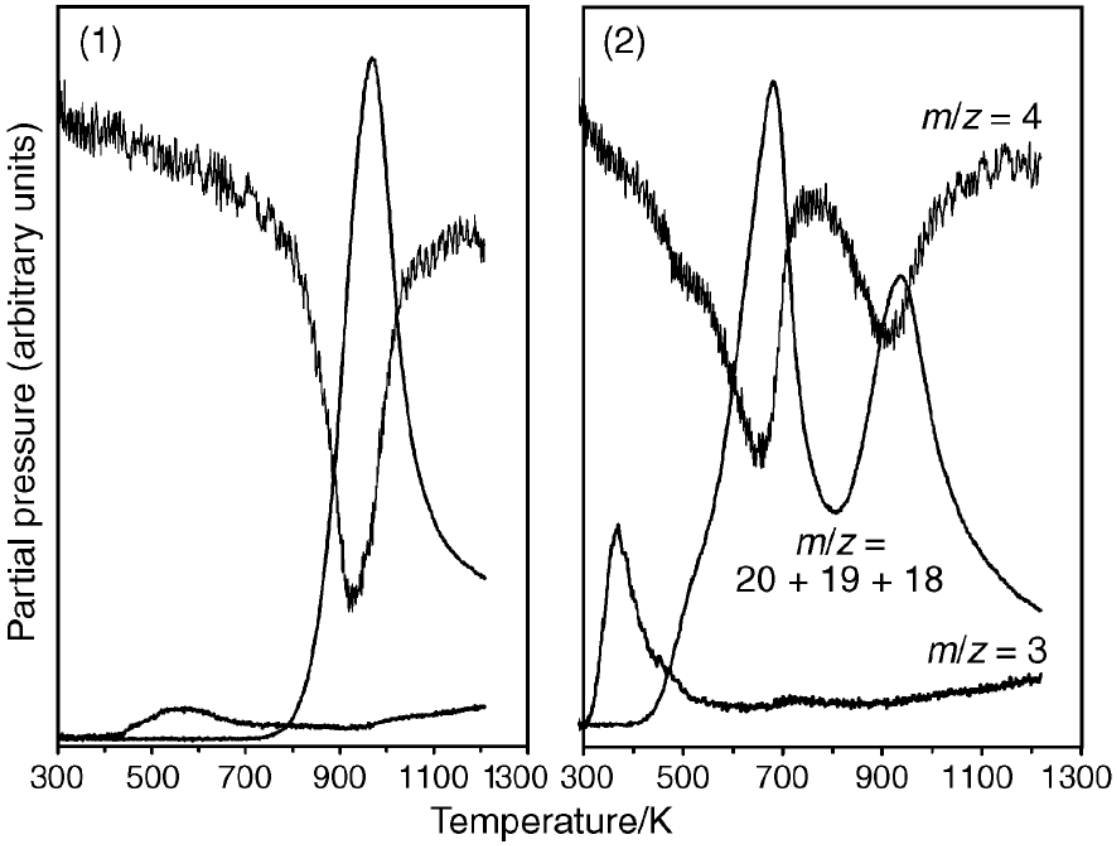
(1)
(2)
m/z = 4
m/z =
20 + 19 + 18
m/z = 3
Partial pressure (arbitrary units)
300
500
700
900
1100
1300
Temperature/K

Fig. 9

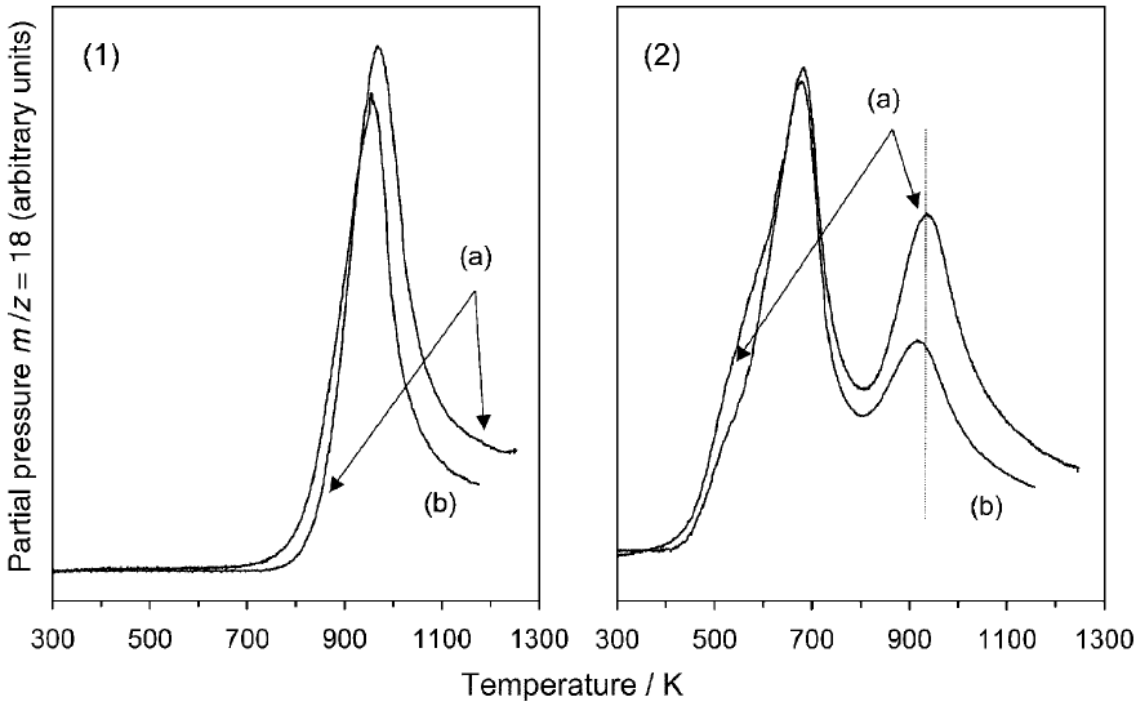
(1)
(2)
(a)
(b)
(a)
(b)
Partial pressure m/z = 18 (arbitrary units)
300
500
700
900
1100
1300
300
500
700
900
1100
1300
Temperature / K

Fig. 10

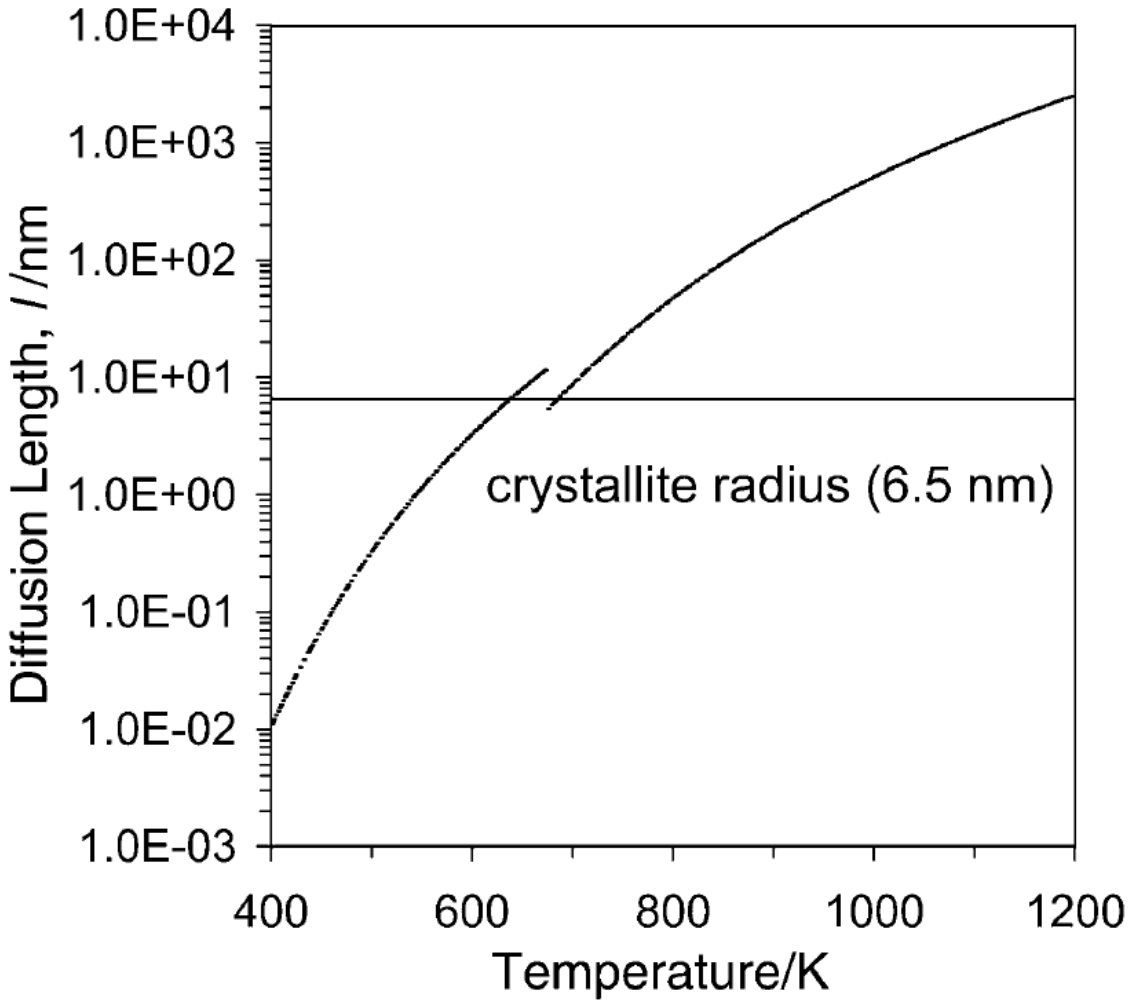
1.0E+04
1.0E+03
1.0E+02
1.0E+01
1.0E+00
1.0E-01
1.0E-02
1.0E-03
Diffusion Length, l /nm
crystallite radius (6.5 nm)
400
600
800
1000
1200
Temperature/K

Fig. 11

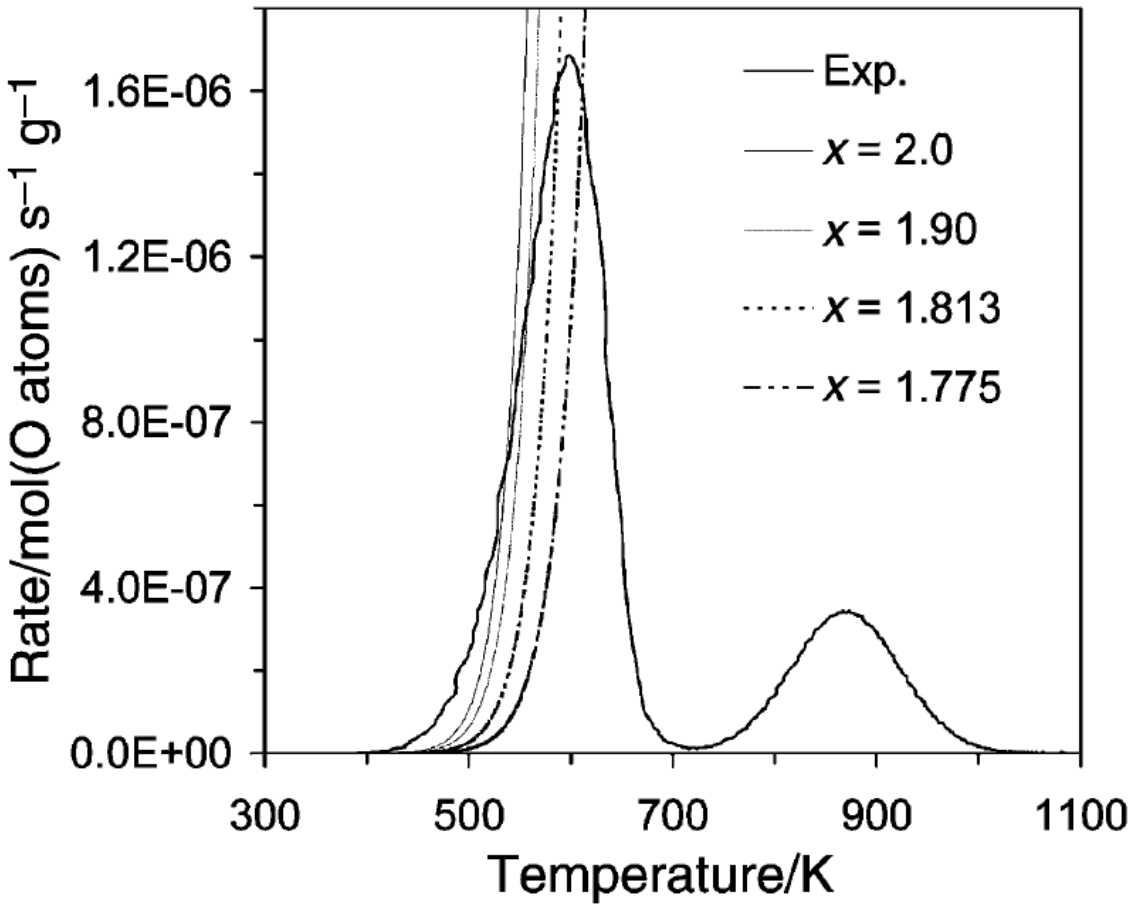
Rate/mol(O atoms) s−1 g−1
1.6E-06
1.2E-06
8.0E-07
4.0E-07
0.0E+00
300
500
700
900
1100
Temperature/K
Exp.
x = 2.0
x = 1.90
x = 1.813
x = 1.775